Weakened energy cascade in elastoinertial turbulence

J. J. J. Gillissen*

Department of Mathematics, University College London, Gower Street, London WC1E 6BT, United Kingdom

(Received 18 December 2020; accepted 21 May 2021; published 21 June 2021)

Newtonian turbulence is characterized by interscale transport of energy from the forcing scales to the dissipation scales. In elastoinertial turbulence, this interscale energy flux is weakened. Here, we explain this phenomenon by numerically showing that elastoinertial energy is predominantly dissipated through polymer chain relaxation. As opposed to Newtonian dissipation, chain relaxation is neither restricted to small nor to large scales but instead it is effective on all the scales. Chain relaxation does not therefore require interscale transport of elastoinertial energy from the forcing scales to the dissipation scales.

DOI: 10.1103/PhysRevE.103.063108

I. INTRODUCTION

In three-dimensional (3D) fluid turbulence, the interscale (i.e., spectral) inertial energy (i.e., kinetic energy) transfer is downscale, i.e., from large to small scales [1], while in two dimensions this transfer is from small to large scales [2]. It is well known that adding polymers modifies this spectral energy transfer. In 3D, polymers weaken the downscale energy transfer [3], which increases the energy at the large scales and reduces the energy at the small scales [4–6]. In two-dimensional (2D) experiments and simulations, polymers have also been observed to weaken the turbulent energy transfer [7,8]. Since in two dimensions, however, the energy transfer is upscale, polymers act to reduce the energy at the large scales and increase the energy at the small scales [9–11].

In this work we conduct 2D and 3D simulations of homogeneous, forced turbulence to further analyze the effects of polymers on the spectral energy transfer. Homogeneous, forced turbulence does not involve walls and the results of this study can therefore not directly be applied to explain the well-known drag reduction effect of polymers on wall bounded flows [12–15].

II. NUMERICAL MODEL

We numerically solve the finitely extensible nonlinear elastic spring model with Peterlin's approximation (FENE-P) [16]:

$$\nabla \cdot \boldsymbol{u} = 0, \tag{1a}$$

$$\partial_t \boldsymbol{u} + \boldsymbol{u}\cdot\nabla\boldsymbol{u} + \frac{1}{\rho}\nabla p = \nu_s \nabla^8 \boldsymbol{u} + \nu_l \nabla^{-2}\boldsymbol{u} + \boldsymbol{f} + \nabla\cdot\boldsymbol{\sigma}, \tag{1b}$$

$$\boldsymbol{\sigma} = \nu_p \lambda^{-1} s(\boldsymbol{c} - \boldsymbol{\delta}), \tag{1c}$$

$$\partial_t \boldsymbol{c} + \boldsymbol{u}\cdot\nabla\boldsymbol{c} - \nabla\boldsymbol{u}^T\cdot\boldsymbol{c} - \boldsymbol{c}\cdot\nabla\boldsymbol{u} = \lambda^{-1}(\boldsymbol{\delta} - s\boldsymbol{c}) + \kappa\sqrt{\boldsymbol{E}:\boldsymbol{E}}\nabla^4\boldsymbol{c}. \tag{1d}$$

Here $\boldsymbol{u}$ is the fluid velocity, p is the fluid pressure, and $\boldsymbol{f} = C_f \sum_{\boldsymbol{k}} \mathrm{Re}\{\boldsymbol{a}(\boldsymbol{k})\exp[-(k-k_f)^2/\Delta k_f^2 + i(\boldsymbol{k}\cdot\boldsymbol{x})2\pi/L]\}$ is the forcing, where $k = |\boldsymbol{k}|$ is the wave number and $\boldsymbol{k}$ is the wave vector. In order to be able to observe both upscale and downscale energy transfer, we force the simulations at intermediate wave numbers, i.e., at length scales that are small compared to the computational domain and large compared to the smallest turbulent structure in the flow. The forcing is spread around the forcing wave number k_f over a wave number interval $\sim\Delta k_f$. The complex forcing amplitude reads $\boldsymbol{a}(\boldsymbol{k}) = \boldsymbol{r}(\boldsymbol{k})\exp[i\phi(\boldsymbol{k})2\pi]$ where $\boldsymbol{r}(\boldsymbol{k})$ and $\phi(\boldsymbol{k})$ are random vectors and numbers (for each $\boldsymbol{k}$) in the interval [0,1]. At each computational time step Δt, a random number $\xi \in [0,1]$ is drawn. If $\xi < \Delta t/t_f$, then $\boldsymbol{r}(\boldsymbol{k})$ and $\phi(\boldsymbol{k})$ are redrawn. This process results in $\boldsymbol{f}$ having a correlation time of t_f. The prefactor C_f is chosen such that $\langle \boldsymbol{f}\cdot\boldsymbol{f}\rangle_x = f_0$, where f_0 is the forcing amplitude and $\langle\cdot\rangle_x$ is the space average.

Equation (1b) contains a high order viscous term (the Laplacian is raised to the fourth power) with ν_s the corresponding solvent hyperviscosity. This hyperviscous term is used instead of the usual viscous stress in order to confine the effect of viscosity to smaller scales. Equation (1b) contains an inverse Laplacian with ν_l the large-scale friction coefficient. This term is added to dissipate energy at the large scales, i.e., to prevent the upscale energy transfer (in 2D simulations) to form vortices that reach the domain size. The ν_l is chosen such that the effect of the large-scale friction is confined to the largest scales.

Equation (1c) defines the polymer stress tensor $\boldsymbol{\sigma}$, where ν_p is the polymer viscosity at zero shear rate, λ is the polymer relaxation time, $\boldsymbol{\delta}$ is the unit tensor, $s = [1 - \mathrm{tr}(\boldsymbol{c})/b]^{-1}$ is the nonlinear spring constant, b is the polymer extensibility parameter, and $\boldsymbol{c}$ is the polymer conformation tensor which is governed by Eq. (1d).

In Eq. (1d) κ is the polymer mass hyperdiffusivity and $\boldsymbol{E} = \frac{1}{2}(\nabla\boldsymbol{u} + \nabla\boldsymbol{u}^T)$ is the rate of strain tensor. By fixing the magnitude of $\kappa \sim \Delta x^4$, the polymer diffusion term $\kappa\sqrt{\boldsymbol{E}:\boldsymbol{E}}\nabla^4\boldsymbol{c}$ suppresses the $\boldsymbol{c}$ modes with wavelengths that are comparable or smaller than the grid spacing $\Delta x = L/N$, with L the domain size and N the number of grid points per dimension.

*jurriaangillissen@gmail.com

Polymer mass diffusivity κ ensures that the numerical scheme produces a smooth solution on the Δx length scale. Although, we show below that, polymer mass diffusivity contributes to 15% of the energy dissipation at very large polymer concentration, the method produces similar physical trends for different grid resolutions and κ [8].

In Eqs. (1a), Newtonian turbulence (NT) is retrieved for zero polymer concentration $\nu_p \to 0$ but also for polymers that behave as passive material lines, i.e., $\lambda \to \infty$ and $b \to \infty$.

We numerically solve Eqs. (1) using Fourier transforms to compute spatial derivatives [8]. Incompressibility [Eq. (1a)] is satisfied by projecting the velocity field on a divergence-free space. Time integration of Eq. (1b) is performed using the explicit, second order Runge-Kutta (RK) scheme with adaptive time stepping. Time integration of Eq. (1d) is performed using RK for the advection, rotation, and stretching terms while the second-order, implicit Crank-Nicolson scheme is used for the relaxation term $\lambda^{-1}(\boldsymbol{\delta} - s\boldsymbol{c})$ [17].

III. 2D SIMULATIONS

For the 2D simulations, we use a domain size $L = 2\pi$, number of grid points $N^2 = 256^2$, solvent hyperviscosity $\nu_s = 0.1\Delta x^8$, large-scale friction coefficient $\nu_l = 0.1$, polymer relaxation time $\lambda = 20$, polymer extensibility parameter $b = 10$, polymer mass hyperdiffusivity $\kappa = \Delta x^4$ for $\nu_p > 10^{-2}$ and $\kappa = 10\Delta x^4$ for $\nu_p < 10^{-2}$, forcing amplitude $f_0 = 10$, forcing wave number $k_f = 16$, forcing wave number range $\Delta k_f = 4$, forcing correlation time $t_f = 0.01$, and we use different values of the polymer viscosity ν_p. In these simulations, the Weissenberg number (based on the rms of the fluctuating rate of strain tensor $\boldsymbol{E}$) $\mathrm{We} = \lambda\sqrt{\langle \boldsymbol{E} : \boldsymbol{E}\rangle_{x,t}}$ is between 10^2 and 10^3, with $\langle\cdot\rangle_{x,t}$ the space-time average. To accumulate accurate statistics, the 2D simulations were integrated to at least 500 simulation time units.

In Fig. 1 we plot, at the latest time of the simulations, the instantaneous fields of the inertial energy density $\frac{1}{2}|\boldsymbol{u}|^2$ and of the elastic energy density $-\frac{1}{2}\nu_p b\lambda^{-1}\ln[1 - \mathrm{tr}(\boldsymbol{c})/b]$ for two different values of $\nu_p = 10^{-5}$ and $\nu_p = 1$. For $\nu_p = 10^{-5}$ the polymers are passively advected and have negligible effect on the velocity field which is close to NT. In this case, most of the inertial energy is contained at the large scales, as evidenced by the large structures in Fig. 1(a). For $\nu_p = 1$, on the other hand, the behavior is referred to as elastoinertial turbulence (EIT). In this case the inertial energy accumulates at the forcing scale $k \sim k_f$. This is evidenced in Fig. 1(b), by the spatial, inertial structures having length scales around L/k_f, which is indicated by the red square. EIT is dominated by elastoinertial shock waves, which were analyzed in detail in Ref. [8]. Movies of these flow structures are provided in the Supplemental Material [18].

Under statistically steady conditions, the governing equations of the inertial energy $K = \frac{1}{2}\langle|\boldsymbol{u}|^2\rangle_{x,t}$ and the elastic energy $P = -\frac{1}{2}\nu_p b\lambda^{-1}\langle\ln[1 - \mathrm{tr}(\boldsymbol{c})/b]\rangle_{x,t}$ are given by

$$0 = F + A - T - D_s - D_l, \tag{2a}$$

$$0 = T + C - R - D_\kappa, \tag{2b}$$

where $F = \langle\boldsymbol{u}\cdot\boldsymbol{f}\rangle_{x,t}$ is the injection rate of inertial energy, $A = \frac{1}{2}\langle\nabla\cdot\boldsymbol{u}|\boldsymbol{u}|^2\rangle_{x,t}$ is the advection of kinetic energy,

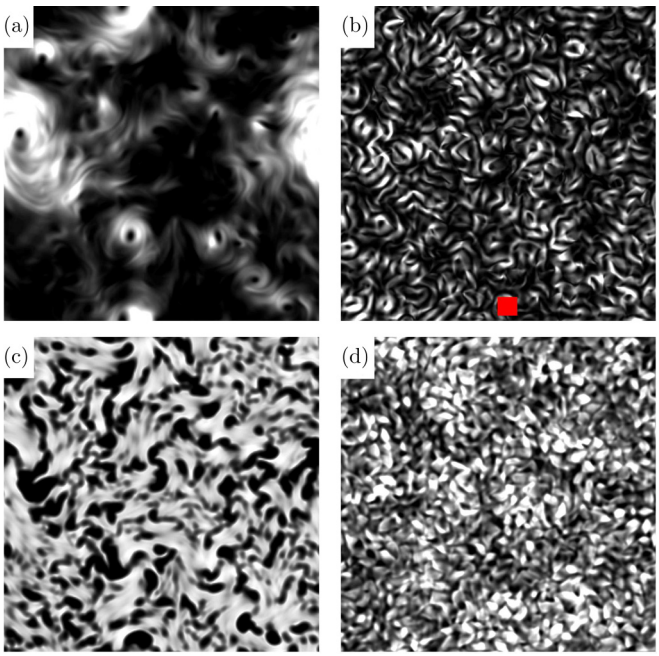

FIG. 1. Visualizations (white is large and black is small) of the inertial energy density (a),(b) and elastic energy density (c),(d) for nearly Newtonian turbulence (NT) with $\nu_p = 10^{-5}$ (a),(c) and elastoinertial turbulence (b),(d) with $\nu_p = 1$ (right). The red square in (b) corresponds to the forcing length scale L/k_f.

$D_s = \nu_s\langle\nabla\boldsymbol{u} : \nabla^7\boldsymbol{u}\rangle_{x,t}$ is the viscous dissipation rate of K at small scales, $D_l = \nu_l\langle\nabla\boldsymbol{u} : \nabla^{-3}\boldsymbol{u}\rangle_{x,t}$ is the dissipation rate of K at large scales, $T = \langle\nabla\boldsymbol{u} : \boldsymbol{\sigma}\rangle_{x,t}$ is the elastoinertial transformation between inertial and elastic energy, $C = -\frac{1}{2}\nu_p b\lambda^{-1}\langle\nabla\cdot\boldsymbol{u}\ln[1 - \mathrm{tr}(\boldsymbol{c})/b]\rangle_{x,t}$ is the advection of elastic energy, $R = \frac{1}{2}\lambda^{-1}\langle\mathrm{tr}(\boldsymbol{\sigma})[1 - \mathrm{tr}(\boldsymbol{c})/b]^{-1}\rangle_{x,t}$ is the dissipation rate of P through conformational diffusion, referred to as polymer relaxation, and $D_\kappa = \frac{1}{2}\nu_p\lambda^{-1}\kappa\langle\sqrt{\boldsymbol{E} : \boldsymbol{E}}[1 - \mathrm{tr}(\boldsymbol{c})/b]^{-1}\nabla^4\mathrm{tr}\boldsymbol{c}\rangle_{x,t}$ is the dissipation rate of P through polymer mass (hyper)diffusion. Note that A and C are zero but their transfer spectra [shown in Figs. 3(c) and 3(d) and 5(c) and 5(d) below] are not.

As opposed to Newtonian turbulence, K in polymer solution turbulence is not conserved in the limit of $\nu_s \to 0$, $\nu_l \to 0$, and $f_0 \to 0$. This is due to the elastoinertial transformation T between K and P which can either go from K to P when $T > 0$ or from P to K when $T < 0$. The local sign of T depends on the alignment between the local polymer stress and velocity gradient tensors. The total energy $K + P$ is not conserved either since the polymers dissipate energy through polymer relaxation R.

In Fig. 2(a) we plot the inertial energy K and the elastic energy P normalized by the energy injection rate F, as functions of ν_p. The figure shows a decrease and saturation of K/F with ν_p and an expected linear increase of P/F with ν_p. It is noted that F varies less than 10% with ν_p (not shown).

In Fig. 2(b) we plot the various terms in Eqs. (2) as functions of ν_p. For NT ($\nu_p \to 0$), the energy injection F is mostly transferred towards the large scales and is dissipated by D_l. As ν_p increases, there is a suppression of dissipation at the large

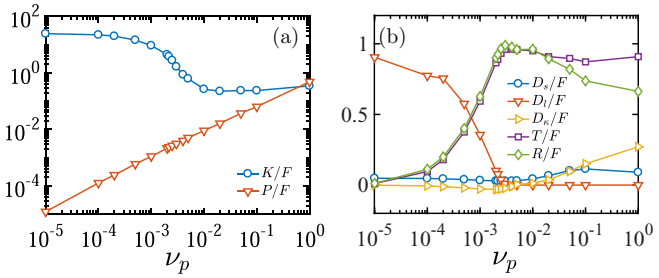

FIG. 2. (a) Inertial and elastic energy. (b) Energy budgets in Eqs. (2).

scales D_l, which implies the suppression of the Newtonian upscale inertial energy transfer.

For EIT ($\nu_p \to 1$), the suppression is complete, i.e., $D_l \to 0$. In this case, the inertial energy K provided by F is transformed into elastic energy P through elastoinertial transformation T and P is subsequently dissipated, mainly through polymer relaxation R. In addition, some portions of K and P are dissipated at the small scales through (hyper)viscosity D_s and through polymer mass (hyper)diffusivity D_κ. These contributions indicate the downscale transfer of K and P, respectively. For $\nu_p = 1$, the dissipation through D_s and D_κ contribute ∼10% and ∼20% to the overall dissipation, respectively.

In Fig. 3 we compare several quantities in wave-number space between nearly NT with $\nu_p = 10^{-5}$ and EIT with $\nu_p = 1$. All variables in Fig. 3 are normalized by F.

In Fig. 3(a) we plot the spectrum $E_K(k)$ of the inertial energy K and the spectrum $E_P(k)$ of the elastic energy P.

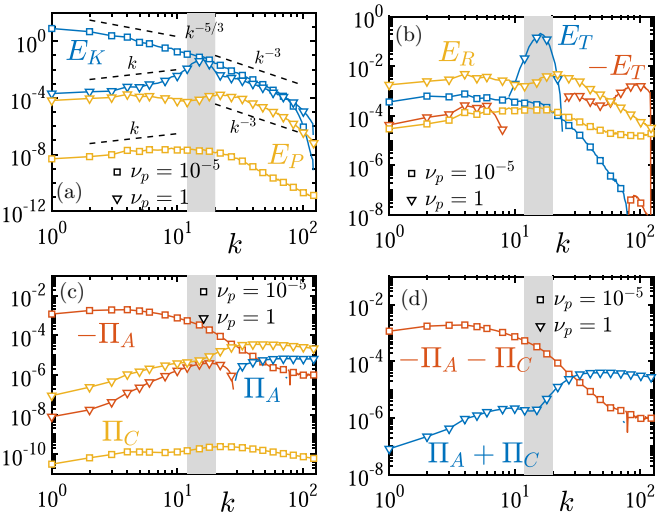

FIG. 3. Comparison of several quantities in wave number k (spectral) space between nearly Newtonian turbulence (NT) with $\nu_p = 10^{-5}$ and elastoinertial turbulence (EIT) with $\nu_p = 1$. All quantities are normalized by F. The gray areas denote the range of wave numbers that are forced, i.e., $k_f - \Delta k_f \leqslant k \leqslant k_f + \Delta k_f$. (a) Inertial and elastic energy. (b) Elastoinertial transformation and polymer relaxation. (c) Advective inertial and elastic energy transfer. (d) Advective total energy transfer. Quantities in (c) and (d) are divided by k.

The exponents for the spectral slopes are only approximate due to the relatively low resolution of the simulations. For $\nu_p = 10^{-5}$, the elastic energy spectrum roughly scales like $E_P(k) \sim k$ for $k \lesssim k_f$ and $E_P(k)$ is somewhat steeper than k^{-3} for $k \gtrsim k_f$. For $\nu_p = 1$, $E_P(k) \sim k^0$ for $k \lesssim k_f$ and $E_P(k) \sim k^{-3}$ for $k \gtrsim k_f$.

For $\nu_p = 10^{-5}$ the inertial energy spectrum roughly follows the Kraichnan-Batchelor scaling laws [2,19], i.e., $E_K(k) \sim k^{-5/3}$ for $k \lesssim k_f$ and $E_K(k) \sim k^{-3}$ for $k \gtrsim k_f$. For $\nu_p = 1$, the upscale inertial energy transfer is suppressed [$D_l \to 0$ in Fig. 2(b)] and $E_K(k)$ has a peak at $k \sim k_f$. This entails that the length scales of the dominant inertial structures are set by the forcing which is also observed in Fig. 1(b). Moreover, for $\nu_p = 1$, $E_K(k)$ for $k \lesssim k_f$ changes from $E_K(k) \sim k^{-5/3}$ to $E_K(k) \sim k$, which is related to the polymer induced suppression of the upscale inertial energy transfer [$D_l \to 0$ in Fig. 2(b)].

In Fig. 3(b) we plot the spectra $E_T(k)$ of the elastoinertial transformation T and the spectra $E_R(k)$ of the polymer relaxation R. For $\nu_p = 10^{-5}$, $E_T(k)$ is predominantly positive, i.e., polymers extract energy from K. For $\nu_p = 1$, large positive values of $E_T(k)$ are concentrated around $k \sim k_f$ while $E_T(k)$ takes small negative values for wave numbers away from $k \sim k_f$. For $k \lesssim k_f$, $E_T(k)$ is of the order of 10^{-4}. This suggests that the large scales of the velocity field are not affected by elastoinertial transformation T.

For both $\nu_p = 10^{-5}$ and $\nu_p = 1$, $E_R(k)$ follows the shape of $E_P(k)$ [Fig. 3(a)], which has a (mild) peak at $k \sim k_f$. The similarity between chain relaxation $E_R(k)$ and elastic energy $E_P(k)$ follows from the $b \to \infty$ limit of the definitions of $P \sim \mathrm{tr}\boldsymbol{c}$ and $R \sim \mathrm{tr}\boldsymbol{\sigma} \sim \mathrm{tr}\boldsymbol{c}$, given above. This similarity $E_R(k) \sim E_P(k)$ suggests that the EIT energy dissipation is effective on all the scales of the energy spectrum. This explains that 2D EIT does not cascade energy to the large dissipative scales. The situation is in stark contrast to the 2D Newtonian turbulence simulation where the dissipation due to the inverse viscous stress scales inversely with the wave number $E_{D_l}(k) \sim k^{-2}E_K(k)$ and the energy is transferred from the forcing scale to the large dissipative scales.

To further study the nature of interscale energy transfer, we plot in Fig. 3(c) the spectral advective flux of inertial energy $\Pi_A(k)$ and that of elastic energy $\Pi_C(k)$:

$$\Pi_A = \tfrac{1}{2}\mathrm{Re}\langle i\boldsymbol{k}\cdot\widehat{\boldsymbol{u}\boldsymbol{u}\cdot\boldsymbol{u}}^*\rangle_{t,k}, \tag{3a}$$

$$\Pi_C = -\tfrac{1}{2}\nu_p b\lambda^{-1}\mathrm{Re}\langle i\boldsymbol{k}\cdot\widehat{\boldsymbol{u}}\,\widehat{\ln[1-\mathrm{tr}(\boldsymbol{c})/b]}^*\rangle_{t,k}. \tag{3b}$$

Here $i = \sqrt{-1}$ is the imaginary unit, $\widehat{\cdot}$ is the spatial Fourier transform, $\cdot^*$ is the complex conjugate, Re is the real part, and $\langle v\rangle_{t,k} = \int_{|\boldsymbol{k}'|\leqslant k}\langle v(\boldsymbol{k}')\rangle_t d^2\boldsymbol{k}'$ is an integral in wave-vector space of the time average $\langle v\rangle_t$ of a variable v. Positive and negative values correspond to downscale and upscale energy fluxes, respectively. Downscale transport is predominantly confined to $k \gtrsim k_f$, while upscale transport is predominantly confined to $k \lesssim k_f$.

Figure 3(c) shows that the elastic energy is transferred downscale, i.e., $\Pi_C(k) > 0$ predominantly for $k \gtrsim k_f$ and the transfer rate increases with ν_p. Inertial energy, on the other hand, is transferred upscale for $\nu_p = 10^{-5}$, i.e., $\Pi_A(k) < 0$ predominantly for $k \lesssim k_f$.

The magnitude of $\Pi_A(k)$ decreases with ν_p and eventually $\Pi_A(k)$ changes from upscale to downscale, i.e., $\Pi_A(k) > 0$ for $k \gtrsim k_f$. For $\nu_p = 1$, there is negligible $\Pi_A(k)$ in the large scales $k \lesssim k_f$, which is consistent with $D_l \to 0$ in Fig. 2(b). Negligible D_l [Fig. 2(b)], negligible $E_T(k)$ [Fig. 3(b)], and negligible Π_K [Fig. 3(c)] suggest that E_K is in *absolute equilibrium* for $k \lesssim k_f$ and follows the 2D Euler spectrum $E_K \sim k$ which is approximately observed in Fig. 3(a); see also Refs. [20,21].

In Fig. 3(d), we plot the spectral transfer of the total energy due to advection $\Pi_A(k) + \Pi_C(k)$. For $\nu_p = 10^{-5}$, the advective transfer $\Pi_A(k) + \Pi_C(k)$ is dominated by the upscale transfer of inertial energy $\Pi_A(k) < 0$ for $k \lesssim k_f$. For $\nu_p = 1$ the advective transfer $\Pi_A(k) + \Pi_C(k)$ is dominated by the downscale transfer of elastic energy $\Pi_C(k) > 0$ for $k \gtrsim k_f$.

Note that the (spectral) energy balances are dominated by large-scale friction for $\nu_p = 10^{-5}$ and by polymer relaxation for $\nu_p = 1$, while the advective terms only contribute to about 1% of the (spectral) energy balances, in both cases. This is reflected by the relatively small values for $\Pi_A(k) + \Pi_C(k)$ in Fig. 3(d).

IV. 3D SIMULATIONS

Next we study the spectral energy transfer in three dimensions. To this end, we have conducted one simulation of NT with polymer viscosity $\nu_p = 10^{-5}$ and one simulation of EIT with $\nu_p = 1$. Parameters are the same as for the 2D simulations, except for the number of grid points $N^3 = 128^3$, the forcing wave number $k_f = 12$, and the forcing wave-number range $\Delta k_f = 2$. The 3D simulations are run for 60 time units to reach a statistically steady state and statistics are collected between $60 < t < 70$.

As shown in Table I, we find that NT dissipates all its energy through small-scale viscosity $D_s/F = 1$, and to a negligible extent through large-scale viscosity $D_l/F = 1 \times 10^{-3}$, polymer chain relaxation $R/F = 6 \times 10^{-4}$, and polymer mass diffusion $D_\kappa/F = 1 \times 10^{-4}$. This confirms that, in 3D NT, energy is transferred to small scales where it is dissipated. EIT, on the other hand, dissipates its energy mainly through polymer chain relaxation $R/F = 0.83$ and to a lesser extent through polymer mass diffusion $D_\kappa/F = 0.15$ and small-scale viscosity $D_s/F = 5 \times 10^{-2}$, and to a negligible extent through large-scale viscosity $D_l/F = 3 \times 10^{-4}$. This suggests that

TABLE I. Statistics of the 3D simulations. Quantities are defined below Eq. (2).

RUN	NT	EIT
ν_p	10^{-5}	1
K/F	1.4	0.44
P/F	9.5×10^{-6}	0.51
D_l/F	1.0×10^{-3}	3.4×10^{-4}
D_s/F	1.0	5.4×10^{-2}
D_κ/F	1.0×10^{-4}	0.15
R/F	5.5×10^{-4}	0.83
T/F	6.5×10^{-4}	0.94

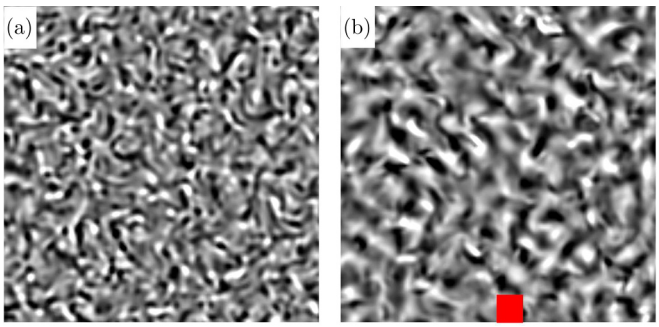

FIG. 4. Visualization of the vorticity component normal to the visualization plane at $t = 70$ for NT (a) and EIT (b). The red square in (b) corresponds to the forcing length scale L/k_f.

in 3D EIT energy is mainly dissipated at the forcing scale through R, while a small fraction of energy is transported to small scales and dissipated through $D_\kappa + D_s$ while an even smaller fraction is transported to large scales and dissipated through D_l.

Figure 4 shows contour plots of the vorticity component normal to the visualization plane at $t = 70$. Figure 4(a) shows that in 3D NT the vorticity is concentrated at the small scales, which is in accordance with the notion that in 3D NT, energy is transported from the forcing scale to the small scales, where it is dissipated. In 3D EIT, on the other hand, the dominant vorticity length scale coincides with the forcing scale L/k_f, which is indicated by the red square in Fig. 4(b). This suggests that the spectral energy transfer is weakened, which is consistent with the finding in Table I that small-scale energy dissipation by viscosity is weakened in 3D EIT.

Figure 5(a) shows the spectrum of the inertial energy E_K and that of the elastic energy E_P. Compared to NT the inertial energy is smaller in EIT. In addition, the peak of E_K at k_f is more pronounced in EIT than in NT, which supports a weakened energy transport to small scales. This is further supported by the more negative slope of E_K for $k > k_f$.

Figure 5(b) shows the spectrum of the dissipation due to polymer relaxation E_R and that of elastoinertial transformation E_T. In NT inertial energy is transformed into elastic energy $E_T > 0$ over the entire wave-number range. For EIT this transformation only occurs at $k \sim k_f$ while the transformation is in the opposite direction $E_T < 0$ away from k_f. For both NT and EIT, the spectra of polymer relaxation E_R follow that of the elastic energy E_P [Fig. 5(a)], i.e., they are evenly distributed over the entire wave-number range, with a mild peak at $k \sim k_f$. This spectral dissipation behavior is fundamentally different to that by mass or momentum diffusion, which are concentrated at large wave numbers (not shown).

Figure 5(c) shows the spectral advective flux of inertial energy $\Pi_A(k)$ and that of elastic energy $\Pi_C(k)$ [Eqs. (3)]. The energy flux in NT is dominated by $\Pi_A(k)$ while that in EIT is dominated by $\Pi_C(k)$. In NT, the inertial flux is downscale $\Pi_A > 0$ for the entire wave-number range, while the elastic flux is upscale $\Pi_C < 0$ for $k > k_f$ and downscale $\Pi_C > 0$ for $k < k_f$. In EIT, we remarkably find that the inertial flux is upscale $\Pi_A < 0$ for $k > k_f$ and downscale $\Pi_A > 0$ for $k < k_f$, while the elastic flux is upscale $\Pi_C < 0$ for the entire wave-number range.

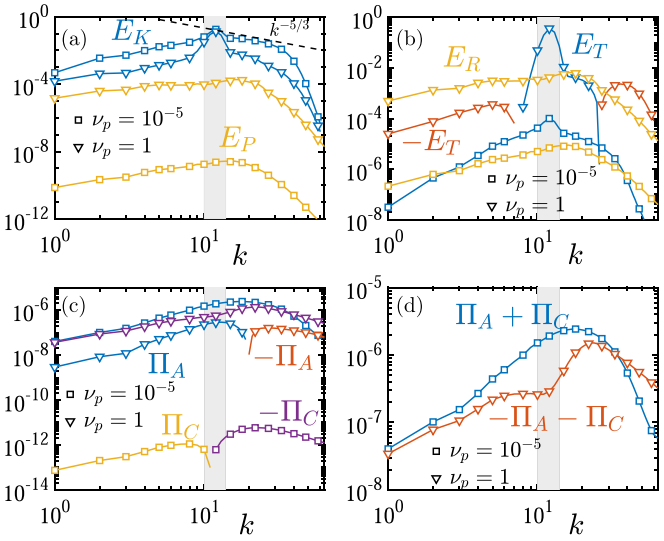

FIG. 5. Comparison of several quantities in wave number k (spectral) space between Newtonian turbulence (NT) with $\nu_p = 10^{-5}$ and elastoinertial turbulence (EIT) with $\nu_p = 1$. All quantities are normalized by F. The gray areas denote the range of wave numbers that are forced, i.e., $k_f - \Delta k_f \leqslant k \leqslant k_f + \Delta k_f$. (a) Inertial energy E_K and elastic energy E_P. (b) Elastoinertial transformation E_T and dissipation by polymer relaxation E_R. (c) Advective inertial energy transfer Π_A and advective elastic energy transfer Π_C. (d) Advective total energy transfer $\Pi_A + \Pi_C$. Quantities in (c) and (d) are scaled by k^2.

Figure 5(d) shows the spectral transfer due to advection of the total (inertial and elastic) energy $\Pi_A(k) + \Pi_C(k)$. Compared to NT, the energy flux in EIT is one order of magnitude smaller for $k \sim k_f$, and the direction is reversed from downscale to upscale over the entire wave-number range.

It is therefore concluded that, similar as in 2D, the energy in 3D EIT is predominantly dissipated by polymer chain relaxation which is broadly distributed spectrally, i.e., not confined to the small dissipation scales. Furthermore, similar as in 2D, the spectral energy transfer in 3D EIT is weakened. In contrast to 2D however, the *direction* of the spectral transfer changes from forward in 3D NT to weakly backward in 3D EIT.

V. CONCLUSION

We have simulated isotropically forced 2D and 3D turbulent polymer solutions using the FENE-P model. For large polymer concentrations, the energy is predominantly dissipated by polymer chain relaxation. In contrast to Newtonian dissipation which in 2D and in 3D acts at the large and small scales, respectively, this polymer dissipation mechanism acts on all scales and does not involve an energy cascade from the forcing scale to these so-called dissipative scales. In accordance to this, the interscale energy transfer is weakened.

ACKNOWLEDGMENTS

We acknowledge the Engineering and Physical Sciences Research Council of the United Kingdom for financial support through Grant No. EP/N024915/1 and Vassilios Dallas for suggesting to simulate EIT with intermediate scale forcing.

[1] A. Kolmogorov, The local structure of turbulence in incompressible viscous fluid for very large Reynolds' numbers, Akad. Nauk SSSR Dokl. **30**, 301 (1941).
[2] R. H. Kraichnan, Inertial ranges in two-dimensional turbulence, Phys. Fluids **10**, 1417 (1967).
[3] P. C. Valente, C. B. da Silva, and F. T. Pinho, Energy spectra in elasto-inertial turbulence, Phys. Fluids **28**, 075108 (2016).
[4] J. M. J. Den Toonder, M. A. Hulsen, G. D. C. Kuiken, and F. T. M. Nieuwstadt, Drag reduction by polymer additives in a turbulent pipe flow: Numerical and laboratory experiments, J. Fluid Mech. **337**, 193 (1997).
[5] Eric van Doorn, Christopher M. White, and K. R. Sreenivasan, The decay of grid turbulence in polymer and surfactant solutions, Phys. Fluids **11**, 2387 (1999).
[6] E. De Angelis, C. M. Casciola, R. Benzi, and R. Piva, Homogeneous isotropic turbulence in dilute polymers, J. Fluid Mech. **531**, 1 (2005).
[7] Anupam Gupta, Prasad Perlekar, and Rahul Pandit, Two-dimensional homogeneous isotropic fluid turbulence with polymer additives, Phys. Rev. E **91**, 033013 (2015).
[8] J. J. J. Gillissen, Two-Dimensional Decaying Elastoinertial Turbulence, Phys. Rev. Lett. **123**, 144502 (2019).
[9] G. Boffetta, A. Celani, and S. Musacchio, Two-Dimensional Turbulence of Dilute Polymer Solutions, Phys. Rev. Lett. **91**, 034501 (2003).
[10] H. Kellay, Polymers suppress the inverse transfers of energy and the enstrophy flux fluctuations in two-dimensional turbulence, Phys. Rev. E **70**, 036310 (2004).
[11] Y. Jun, J. Zhang, and X.-L. Wu, Polymer Effects on Small- and Large-Scale Two-Dimensional Turbulence, Phys. Rev. Lett. **96**, 024502 (2006).
[12] P. S. Virk, Drag reduction fundamentals, AIChE J. **21**, 625 (1975).
[13] D. Samanta, Y. Dubief, M. Holzner, C. Schäfer, A. N. Morozov, C. Wagner, and B. Hof, Elasto-inertial turbulence, Proc. Natl. Acad. Sci. USA **110**, 10557 (2013).
[14] G. H Choueiri, J. M. Lopez, and B. Hof, Exceeding the Asymptotic Limit of Polymer Drag Reduction, Phys. Rev. Lett. **120**, 124501 (2018).
[15] Jose M. Lopez, George H. Choueiri, and Björn Hof, Dynamics of viscoelastic pipe flow at low Reynolds numbers in the maximum drag reduction limit, J. Fluid Mech. **874**, 699 (2019).
[16] R. Byron Bird, Robert C. Armstrong, and Ole Hassager, *Dynamics of Polymeric Liquids* (Wiley, New York, 1987).
[17] P. K. Ptasinski, B. J. Boersma, F. T. M. Nieuwstadt, M. A. Hulsen, B. H. A. A. Van den Brule, and J. C. R. Hunt, Turbulent channel flow near maximum drag reduction: Simulations, experiments and mechanisms, J. Fluid Mech. **490**, 251 (2003).

[18] See Supplemental Material at http://link.aps.org/supplemental/10.1103/PhysRevE.103.063108 for a movie of the flow structures in Newtonian turbulence and in elastoinertial turbulence.

[19] George K. Batchelor, Computation of the energy spectrum in homogeneous two-dimensional turbulence, Phys. Fluids **12**, II–233 (1969).

[20] Vassilios Dallas, Stephan Fauve, and Alexandros Alexakis, Statistical Equilibria of Large Scales in Dissipative Hydrodynamic Turbulence, Phys. Rev. Lett. **115**, 204501 (2015).

[21] Moritz Linkmann and Vassilios Dallas, Large-scale dynamics of magnetic helicity, Phys. Rev. E **94**, 053209 (2016).